

Retrieval-Augmented Diffusion Models

Andreas Blattmann* Robin Rombach* Kaan Oktay Björn Ommer
 University of Munich & IWR, Heidelberg University, Germany

Abstract

Generative image synthesis with diffusion models has recently achieved excellent visual quality in several tasks such as text-based or class-conditional image synthesis. Much of this success is due to a dramatic increase in the computational capacity invested in training these models. This work presents an alternative approach: inspired by its successful application in natural language processing, we propose to complement the diffusion model with a retrieval-based approach and to introduce an explicit memory in the form of an external database. During training, our diffusion model is trained with similar visual features retrieved via CLIP and from the neighborhood of each training instance. By leveraging CLIP’s joint image-text embedding space, our model achieves highly competitive performance on tasks for which it has not been explicitly trained, such as class-conditional or text-image synthesis, and can be conditioned on both text and image embeddings. Moreover, we can apply our approach to unconditional generation, where it achieves state-of-the-art performance. Our approach incurs low computational and memory overheads and is easy to implement. We discuss its relationship to concurrent work and will publish code and pretrained models soon.

1 Introduction

The field of deep generative models has made tremendous leaps; especially in language modeling as well as in generative synthesis of high-fidelity images and other data types. In particular in image synthesis, astounding results have recently been achieved [14, 11, 39, 42], and three main factors can be identified as the driving forces behind this progress: First, the success of the transformer [60] has caused an architectural revolution in many vision tasks [12], for image synthesis especially through its combination with autoregressive modeling [14, 41]. Second, since their rediscovery, diffusion models have been successfully applied to high-resolution image generation [52, 54, 21] and, within a very short time, set new standards in generative image modeling [11, 22, 44, 42]. Third, these approaches *scale* well [42, 25, 56]; in particular when considering the model- and batch sizes involved for high-quality diffusion models [11, 39, 42] there is evidence that this scalability is of central importance for their performance.

However, while performance can most likely be further improved by simply adding more computational power and parameters [56], we here present an orthogonal approach and boost performance of generative image models *without* increasing their mere parameter count. Conversely, inspired by the recent success of retrieval-augmented generative language models [2], we trade off trainable

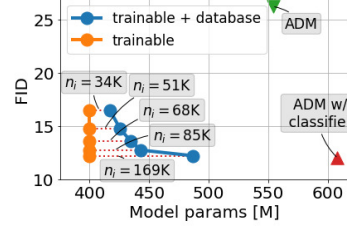


Figure 1: Our model outperforms the recent unconditional SOTA model ADM [11] on ImageNet [10] and reaches its performance when using class labels (ADM w/ classifier), while significantly reducing parameter count. n_i : Number instances in database during inference.

*Equal contribution.

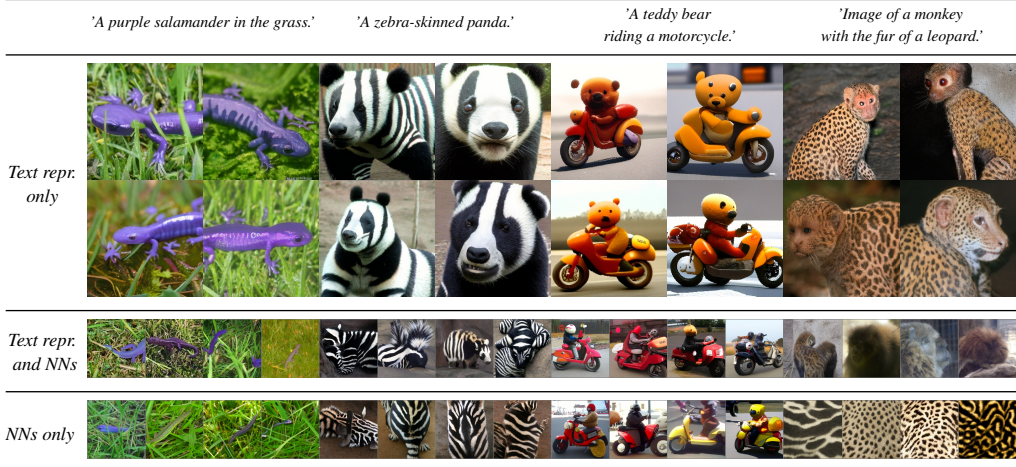


Figure 2: As we retrieve nearest neighbors in the shared text-image space provided by CLIP, we can use text prompts as queries for exemplar-based synthesis. We observe our ImageNet model to readily generalize to unseen/fictional text prompts when building the set of retrieved neighbors by directly conditioning on the CLIP text encoding $\phi_{\text{CLIP}}(c_{\text{text}})$ (top row). When using $\phi_{\text{CLIP}}(c_{\text{text}})$ together with its $k - 1$ nearest neighbors from the retrieval database or the k nearest neighbors alone without the text representation, the model does not show these generalization capabilities (mid- and bottom rows).

parameters for a memory of visual examples and *explicitly* define part of our proposed model by means of an image database. During training, our resulting retrieval-augmented *semi-parametric* model accesses the database via a nearest neighbor lookup and learns to synthesize images based on retrieved visual building blocks. By combining this retrieval-enhanced strategy with a diffusion-based generator, we obtain a lightweight model which nonetheless outperforms its fully parametric counterparts, especially on complex, multi-modal datasets, *cf.* Fig. 1. Moreover, since both database and retrieval strategy are interchangeable after training, our approach can be flexibly applied to conditional tasks such as a text-to-image synthesis as in Fig. 2, despite being trained on images only.

In summary, we present a simple framework for retrieval-augmented generative modeling with diffusion models. By searching in and conditioning on the latent space of CLIP [40], we present an efficient way of incorporating nearest neighbor representations with very little computational overhead. In particular, retrieval is fast (0.95 ms to retrieve 20 nearest neighbors from a database of 20M examples) and conditioning on CLIP embeddings requires little additional storage space (2GB per 1M examples). We show that the semi-parametric approach yields high fidelity and diverse samples; surpassing recent state-of-the-art diffusion models in terms of FID and diversity while requiring less trainable parameters. Furthermore, the shared image-text feature space of CLIP allows for various conditional applications such as text-to-image or class-conditional synthesis, despite being trained on images only (see *e.g.* Fig. 2). Finally, we demonstrate how changing the retrieval database at test time provides additional flexibility in the control the synthesis process and can be combined with existing sampling techniques such as classifier-free diffusion guidance [20].

2 Related Work

Diffusion Models for Image Synthesis. Starting with the seminal works of Sohl-Dickstein et al. [52] and Ho et al. [21], diffusion-based generative models have improved generative modeling of artificial visual systems [11, 31, 61, 23, 64, 46] and other data [32, 24, 62] by sequentially removing noise from a random signal to generate an image. Being likelihood-based models, they achieve high data distribution coverage with well-behaved optimization properties while producing high resolution images at unprecedented quality. Furthermore, the performance of diffusion models follows a predictable trend when scaling the number of parameters, as demonstrated by Dhariwal et al. [11]. Their good performance, however, comes at the expense of high training costs and slow sampling. Different approaches have been proposed to circumvent these drawbacks, either via shortened denoising schedules [53, 58, 35, 61], distillation [37, 47] or two-stage modeling [44, 51, 13]. However, they still require large models and significant compute resources, especially for

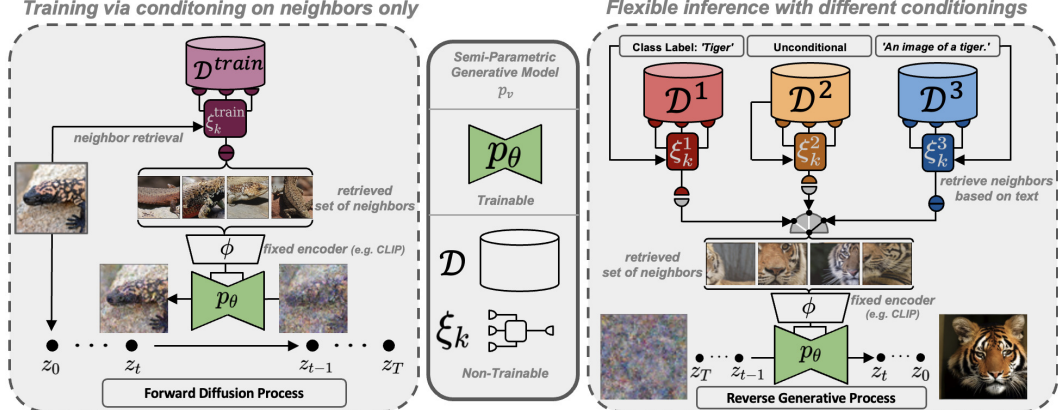


Figure 3: Our retrieval-augmented, semi-parametric diffusion model consists of a trainable conditional generative decoding head $p(x|\cdot)$, a database \mathcal{D} containing visual examples and a sampling strategy ξ_k to obtain a subset $\mathcal{M}_{\mathcal{D}}^{(k)} \subseteq \mathcal{D}$, which serves as conditioning for p_{θ} . During training (left), ξ_k^{train} retrieves the nearest neighbors of each target example from \mathcal{D} , such that p_{θ} only needs to learn to compose consistent scenes based on $\mathcal{M}_{\mathcal{D}}^{(k)}$, cf. Sec 3.2. During inference (right), we can interchange \mathcal{D} and ξ_k , thus resulting in flexible sampling capabilities such as post-hoc conditioning on class labels (ξ_k^1) or text prompts (ξ_k^3), cf. Sec. 3.3.

unconditional image generation [11] on complex datasets like ImageNet [10] or complex conditional tasks such as text-to-image generation [39, 16, 44].

To address these issues, given limited compute resources, and inspired by previous work in natural language processing [2], we propose to trade trainable parameters for an external memory which empowers smaller models to achieve high fidelity image generation on par with ever-growing models.

Retrieval-Augmented Generative Models. Using external memory to augment traditional models has recently drawn attention in natural language processing (NLP) [29, 30, 38, 18]. For example, RETRO [2] proposes a retrieval-enhanced transformer for language modeling which performs on par with state-of-the-art models [4] using significantly less parameters and compute resources. These retrieval-augmented models with external memory turn purely parametric deep learning models into semi-parametric ones. Early attempts [36, 50, 57, 63] in retrieval-augmented visual models do not use an external memory and exploit the training data itself for retrieval. In image synthesis, IC-GAN [5] utilizes the neighborhood of training images to train a GAN and generates samples by conditioning on single instances from the training data. However, using training data itself for retrieval potentially limits the generalization capacity, and thus, we favor an external memory in this work.

Concurrent Work Very recently, two concurrent approaches related to our work, unCLIP [42] and kNN-Diffusion [1], have been proposed. unCLIP produces very high quality text-image results by conditioning a diffusion model on the image representation of CLIP [40] and employing large-scale computation. However, unlike our work, it conditions on the CLIP representation of the training data itself, which makes it necessary to learn a generative text-image prior later. kNN-Diffusion, like our approach, avoids this problem by conditioning on a neighborhood. Although both kNN-Diffusion and our approach are fundamentally very similar, we use a continuous rather than a discrete diffusion formulation, analyze different forms of neighborhood representations, and are not exclusively limited to text-image synthesis.

3 Image Synthesis with Retrieval-Augmented Diffusion Models

Our work considers data points as an explicit *part of the model*. In contrast to common neural generative approaches to image synthesis [3, 28, 49, 43, 14, 7, 6], this approach is not only parameterized by the learnable weights of a neural network, but also a (fixed) set of data representations and a non-learnable *retrieval* function, which, given a query from the training data, retrieves suitable data representations from the internal dataset. Following prior work in natural language modeling [2], we implement this retrieval pipeline as a nearest neighbor lookup.

Sec. 3.1 and Sec. 3.2 formalize this approach for training retrieval-augmented diffusion models for image synthesis, while Sec. 3.3 and Sec. 3.4 introduce flexible sampling mechanisms that become available once such a model is trained. Fig. 3 provides an overview over our approach.

3.1 Retrieval-Enhanced Generative Models of Images

Unlike common, fully parametric neural generative approaches for images, we define a *semi-parametric* generative image model $p_\nu(x)$ by introducing a tuple of trainable *and* non-trainable model components $\nu = \{\theta, \mathcal{D}, \xi_k\}$, where $\mathcal{D} = \{y_i\}_{i=1}^N$ is a *fixed* database of images $y_i \in \mathbb{R}^{H_D \times W_D \times 3}$. Further, ξ_k denotes a (non-trainable) sampling strategy to obtain a subset of \mathcal{D} based on a query x , i.e. $\xi_k : x, \mathcal{D} \mapsto \mathcal{M}_\mathcal{D}^{(k)}$, where $\mathcal{M}_\mathcal{D}^{(k)} \subseteq \mathcal{D}$ and $|\mathcal{M}_\mathcal{D}^{(k)}| = k$. Thus, only θ is actually learned during training.

Importantly, $\xi_k(x, \mathcal{D})$ has to be chosen such that it provides the model with beneficial visual representations from \mathcal{D} for modeling x and the entire capacity of θ can be leveraged to *compose* consistent scenes based on these patterns. For instance, considering query images $x \in \mathbb{R}^{H_x \times W_x \times 3}$, a valid strategy $\xi_k(x, \mathcal{D})$ is a function that for each x returns the set of its k nearest neighbors, measured by a given distance function $d(x, \cdot)$.

Next, we propose to provide this retrieved information to the model via *conditioning*, i.e. we specify a general semi-parametric generative model as

$$p_{\theta, \mathcal{D}, \xi_k}(x) = p_\theta(x | \{y | y \in \xi_k(x, \mathcal{D})\}) = p_\theta(x | \{y | y \in \mathcal{M}_\mathcal{D}^{(k)}\}) \quad (1)$$

In principle, one could directly use image samples $y \in \mathcal{M}_\mathcal{D}^{(k)}$ to learn θ . However, since images contain many ambiguities and their high dimensionality involves considerable computational and storage cost² we use a *fixed*, pre-trained image encoder ϕ to project all examples from $\mathcal{M}_\mathcal{D}^{(k)}$ onto a low-dimensional manifold. Hence, Eq. (1) reads

$$p_{\theta, \mathcal{D}, \xi_k}(x) = p_\theta(x | \{\phi(y) | y \in \xi_k(x, \mathcal{D})\}). \quad (2)$$

where $p_\theta(x | \cdot)$ is a conditional generative model with trainable parameters θ which we refer to as *decoding head*. With this, the above procedure can be applied to any type of generative decoding head and is not dependent on its concrete training procedure.

3.2 Semi-Parametric Diffusion Models

During training we are given a train dataset $\mathcal{X} = \{x_i\}_{i=1}^M$ of images whose distribution $p(x)$ we want to approximate with $p_\nu(x)$. Our train-time sampling strategy ξ_k uses a query example $x \sim p(x)$ to retrieve its k nearest neighbors from \mathcal{D} by implementing $d(x, y)$ as the cosine similarity in the image feature space of CLIP [40]. Given a sufficiently large database \mathcal{D} , this strategy ensures that the set of neighbors $\xi_k^{\text{train}}(x, \mathcal{D})$ shares sufficient information with x and, thus, provides useful visual information for the generative task. We choose CLIP to implement ξ_k , because it embeds images in a low dimensional space ($\text{dim} = 512$) and maps semantically similar samples to the same neighborhood, yielding an efficient search space. Fig. 4 visualizes examples of nearest neighbors retrieved via a ViT-B/32 vision transformer [12] backbone.

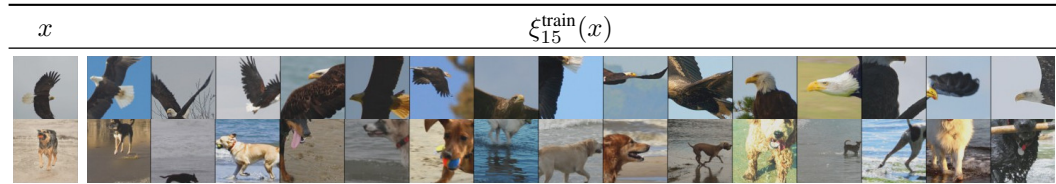


Figure 4: $k = 15$ nearest neighbors from \mathcal{D} for a given query x when parameterizing $d(x, \cdot)$ with CLIP [40].

Note that this approach can, in principle, turn any generative model into a semi-parametric model in the sense of Eq. (2). While this formulation supports various explicit likelihood approaches

²Note that \mathcal{D} is essentially a part of the model weights

such as normalizing flows or autoregressive models, in this work we focus on models where the decoding head is implemented as a diffusion model, motivated by the recent success in diffusion-based image synthesis [21, 11, 44, 39]. In order to reduce computational complexity and memory requirements during training, we follow [44] and use a *latent diffusion model (LDM)* which learns the data distribution in the latent space of a VQGAN-based image compressor $z = E(x)$.

To obtain the image representations via ϕ , different compressor models are conceivable in principle. Again, the latent space of CLIP offers some advantages since it is (i) very compact, which (ii) also reduces memory requirements. Moreover, the contrastive pretraining objective (iii) provides a shared space of image and text representations, which is beneficial for text-image synthesis, as we will show in Sec. 4.2. We draw a comparison to other approaches for ϕ that provide discrete representations in Sec. 4.1. However, unless otherwise specified, $\phi \equiv \phi_{\text{CLIP}}$ is set in the following.

Note that with this choice the additional database \mathcal{D} can also be interpreted as a fixed *embedding layer*³ of dimensionality $|\mathcal{D}| \times 512$ from which the nearest neighbors are retrieved.

We dub this retrieval-augmented diffusion model *RDM* and train it with the usual reweighted likelihood objective [21], yielding the objective [52, 21]

$$\min_{\theta} \mathcal{L} = \mathbb{E}_{p(x), z \sim E(x), \epsilon \sim \mathcal{N}(0, 1), t} \left\{ \|\epsilon - \epsilon_{\theta}(z_t, t, \{\phi_{\text{CLIP}}(y) | y \in \xi_k(x, \mathcal{D})\})\|_2^2 \right\}, \quad (3)$$

where the expectation is approximated by the empirical mean over training examples. In the above equation, ϵ_{θ} denotes the UNet-based [45] denoising autoencoder as used in [11, 44] and $t \sim \text{Uniform}(1, T)$ denotes the time step [52, 21]. To feed the set of nearest neighbor encodings $\phi_{\text{CLIP}}(y)$ into ϵ_{θ} , we use the cross-attention conditioning mechanism proposed in [44].

3.3 Inference for Retrieval-Augmented Diffusion Models

During inference we have no access to query instances from the train set. However, since \mathcal{D} and ξ_k are not learned, we can change them at test time as long as they still provide $p_{\theta}(x|\cdot)$ with a suitable set of visual representations.

Conditional Synthesis without Conditional Training During synthesis, additional conditional information such as text prompts or class labels, which has not been available during training, can provide more fine-grained control. The interchangeability of \mathcal{D} and ξ_k at test time offers additional flexibility compared to standard generative approaches: Depending on the application, it is possible to extent/restrict \mathcal{D} for particular exemplars; or to skip the retrieval via ξ_k altogether and provide a set of representations $\{\phi_{\text{CLIP}}(y_i)\}_{i=1}^k$ directly.

For text-to-image generation, for example, our model can be conditioned in several ways: Given a text prompt c_{text} and using the text-to-image retrieval ability of CLIP, we can retrieve k neighbors from \mathcal{D} and use these as an implicit text-based conditioning. However, since we condition on CLIP representations ϕ_{CLIP} , we can also condition directly on the *text* embeddings obtained via CLIP’s language backbone (since CLIP’s text-image embedding space is shared). Accordingly, it is also possible to combine these approaches and use text and image representations simultaneously. We show and compare the results of using these sampling techniques in Fig. 2.

In the case of a class label c_c , we can define a text such as ‘*An image of a $t(c_c)$.*’ based on its textual description $t(c_c)$, apply the embedding strategy for text prompts and sample a pool $\xi_l(c_c)$, $k \leq l$ for each class. By randomly selecting k adjacent examples from this pool for a given query label c_c , we obtain an inference-time class-conditional model. We experimentally investigate these two cases of post-hoc conditioning in Sec. 4.2.

For **unconditional generative modeling**, we randomly sample a pseudo-query $\tilde{x} \in \mathcal{D}$ and use $\xi_k^{\text{test}} = \xi_k^{\text{train}}$ to obtain the set $\xi_k^{\text{test}}(\tilde{x}, \mathcal{D})$ of its k nearest neighbors. Given this set, Eq. (2) can be used to draw samples, since $p_{\theta}(x|\cdot)$ itself is a generative model. However when generating all samples from $p_{\theta}(x)$ only from one particular set $\xi_k^{\text{test}}(\tilde{x})$, we expect $p_{\theta}(x)$ to be unimodal and sharply peaked around \tilde{x} , *e.g.* the leftmost example in Fig. 11. When intending to model a complex multimodal distribution $p(x)$ of natural images, this choice would obviously lead to weak results. Therefore, we

³For a database of 1M images and using 32-bit precision, this equals approximately 2.048 GB

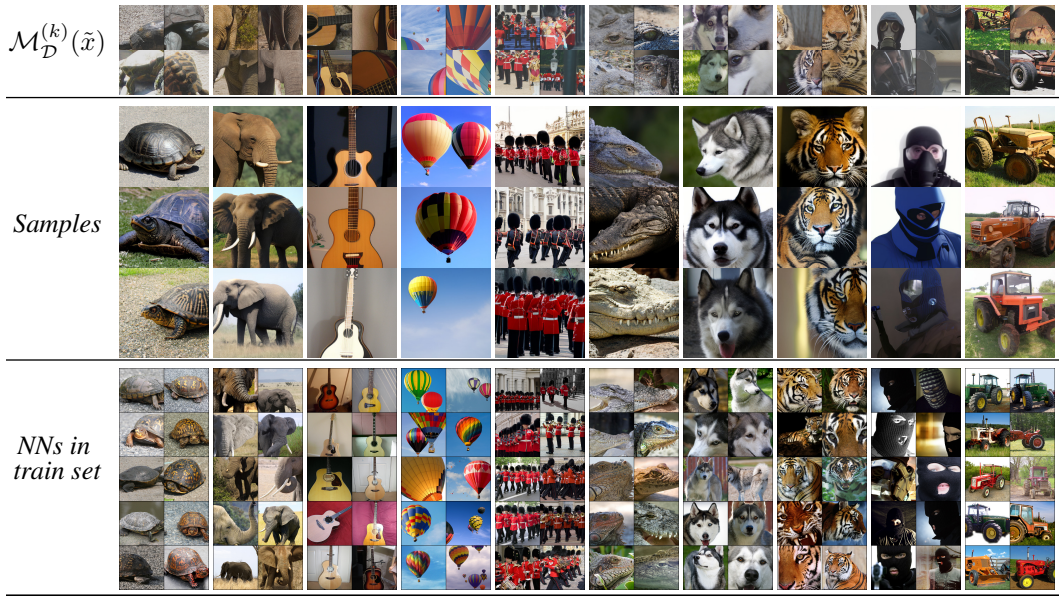


Figure 5: Samples from our unconditional *RDM* together with the set of $\mathcal{M}_\mathcal{D}^{(k)}(\tilde{x})$ of retrieved neighbors based on the pseudo query \tilde{x} , cf. Sec. 3.3 and nearest neighbors from the train set, measured in CLIP [40] feature space. Sample are generated with $m = 0.01$, guidance with $s = 2.0$ and 100 DDIM steps.

construct a proposal distribution $p_{\mathcal{D}}(\tilde{x}) = \sum_{i=1}^{|\mathcal{D}|} p_i \delta(\tilde{x} - x_i)$, where

$$p_i = \frac{1}{k \cdot M} \sum_{x \in \mathcal{X}} \sum_{y \in \xi_k(x, \mathcal{D})} \delta(y - y_i), \quad i = 1, \dots, |\mathcal{D}|.$$

This definition counts the instances in the database \mathcal{D} which are useful for modeling the training dataset \mathcal{X} . Note that, $p_{\mathcal{D}}(\tilde{x})$ only depends on \mathcal{X} and \mathcal{D} , what allows us to precompute it. Given $p_{\mathcal{D}}(\tilde{x})$, we can obtain a set

$$\mathcal{P} = \left\{ p_{\theta}(x | \{\phi(y) | y \in \xi_k(\tilde{x}, \mathcal{D})\}) \mid \tilde{x} \sim p_{\mathcal{D}}(\tilde{x}) \right\} \quad (4)$$

of samples from the our model. We can thus draw from the unconditional modeled density $p_{\nu}(x)$ by drawing $x \sim \text{Uniform}(\mathcal{P})$.

3.4 Trading Quality for Diversity

Many approaches to (conditional) generative modeling offer ways to trade off sample quality for diversity at test time. GANs and diffusion models can achieve this by leveraging conditional information via *truncated sampling* [3] and *classifier guidance* [11, 20], while autoregressive models allow for *top-k sampling* [15].

We propose a similar technique for semi-parametric generative models. Let $Z_m = \sum_{\tilde{x} \in \mathcal{D}^{(m)}} p_{\mathcal{D}}(\tilde{x})$, where $\mathcal{D}^{(m)} \subseteq \mathcal{D}$ is the subset containing the fraction $m \in (0, 1]$ of most likely examples $\tilde{x} \sim p_{\mathcal{D}}(\tilde{x})$. Similar to top-k sampling, we define a truncated distribution

$$\mu(\tilde{x}) = \begin{cases} p_{\mathcal{D}}(\tilde{x})/Z_m, & \text{if } \tilde{x} \in \mathcal{D}^{(m)} \\ 0, & \text{else,} \end{cases} \quad (5)$$

which we can use as proposal distribution to obtain \mathcal{P} according to Eq. (4). Thus, for small values of m , this yields samples from a narrow, almost unimodal distribution. Increasing m on the other hand, increases diversity, potentially at the cost of reduced sample quality. We analyze this trade-off in Sec. 4.3 and Fig. 13. In analogy to top-k sampling, we dub this sampling scheme *top-m sampling*.

To gain additional flexibility during inference, this scheme can further be combined with model-specific sampling techniques such as **classifier-free diffusion guidance** [20], since our model *RDM* is

a conditional diffusion model of the nearest neighbor encodings $\phi(y)$. We present results using different combinations of m and classifier-free guidance scales s in Sec. 4.3.

4 Experiments

This section presents experiments using the retrieval-augmented diffusion model as introduced in Sec. 3. We analyze different retrieval strategies and neighbor representations ϕ in Sec. 4.1, investigate sampling strategies in Sec. 4.3, compare with state-of-the-art methods in Sec. 4.4 and present conditional applications such as text-to-image in Sec. 4.2.

The architecture of our decoding head closely follows the class-conditional ImageNet model of [44]. The only changes are a reduced parameter count from 580M to 400M trainable parameters and the removal of the class embedding layer. For more details regarding model architecture and training, *cf.* Tab. 2.

For all experiments we use a database \mathcal{D} of 20M examples built from the OpenImages [33] dataset. OpenImages contains 9M images with edge lengths of at least 1200 pixels. We extract 2-3 patches per image (see Sec. 4.1) to use each image at least once.

To obtain nearest neighbors we apply the ScaNN search algorithm [17] in the feature space of a pretrained CLIP-ViT-B/32 [40]. Using this setting, retrieving 20 nearest neighbors from the database described above takes approximately 0.95 ms. Thus, including NN retrieval in the training process does not mean significant training time overheads. Since the retrieved neighbors only depend on \mathcal{D} and the train dataset, we pre-compute them to speed up training and save the corresponding representations of the encoder ϕ (*cf.* Sec. 4.1) as this is less hard disk intensive than saving raw images.

For quantitative performance measures we use FID [19], Inception Score (IS) [48] and Precision-Recall [34], and generate samples with the DDIM sampler [53] with 100 steps and $\eta = 1$. Hyperparameters and further evaluation details are included in the Appendix A.1 and A.2.

4.1 Analyzing Retrieval-Augmented Diffusion Models

We first analyze various design decisions for building the semi-parametric diffusion model as described in Sec. 3. To limit computational demands, we use a subset of ImageNet, which consists of all *dog* classes (*cf.* Tab. 3) (163K images), and generate 1000 instead of 50k examples for evaluation.

Following the standard protocol [3, 11], we evaluate against the full training set for quantitative performance metrics (such as FID).

Which representations to use for retrieved neighbors?

Conditioning on raw image pixels would result in excessive memory/storage demands, finding an appropriate compressed representation $\phi(y)$ for the retrieved neighbors $y \in \mathcal{M}_{\mathcal{D}}^{(k)}$ is of central importance. Since many powerful pre-trained feature extractors are readily available, we focus on fixed, pre-trained encoders to obtain the representations $\phi(y)$; it is, however, also possible to learn such a model jointly with the decoder. We investigate two types of representations and compare those from a pre-trained VQGAN encoder [14], representations from the image encoder of CLIP [40]. We use $k = 4$ nearest neighbors for both models.

Fig. 6 summarizes the obtained results which demonstrate the efficacy of semi-parametric generative modeling compared to fully-parametric models, as both VQGAN- and CLIP-nearest-neighbor encodings improve sample quality (higher precision [34], lower FID [19]) as well as diversity (higher recall [34]), despite using less trainable parameters (the baseline uses $1.3 \times$ more parameters). As CLIP encodings consistently lead to improved results compared to VQGAN representations, we use them for all following experiments.

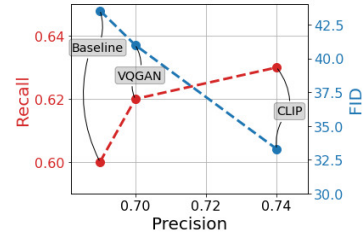


Figure 6: Performance of *RDM* with different nearest neighbor representations.

How many neighbors to retrieve? To answer this question we train five *RDM* with identical decoding heads with the same hyperparameters with different numbers $k \in \{1, 2, 4, 8, 16\}$ of retrieved neighbors during training with a database \mathcal{D} with $H_{\mathcal{D}} = W_{\mathcal{D}} = 128$. To obtain faster convergence we train these models on the dogs-subset of ImageNet on a single A-100 machine and evaluate on 1000 samples. Fig. 7 shows the obtained results. FID and Precision scores indicate that increasing the number of neighbors is actually not beneficial for sample quality. In terms of recall scores, however, we observe that $k = 4$ performs best. As for all k , the visual quality of the samples is generally high, and $k = 4$ gives the highest sample diversity, we use this value for the remaining experiments. Depending on subjective preferences, however, other choices might also be valid.

Should we condition on objects or object parts? We observe that the patch size of the extracted patches in \mathcal{D} has significant impact on the performance of our models. Fig. 8 visualizes performance metrics for three identical *RDM* models, conditioned on CLIP [40] embeddings of $k = 4$ nearest neighbors from databases with different patch sizes $H_{\mathcal{D}} = W_{\mathcal{D}} \in \{64, 128, 256\}$.

Vertical and horizontal bars denote the performance of a *LDM* baseline with $1.3 \times$ more parameters. We see that a patch size of 64 px seems to be too small, resulting in worse performance compared to the baseline. Increasing the patch size results in significant improvements over the baseline, despite a smaller parameter count. High precision [34] and FID [19] indicate that conditioning on larger patches results in improved sample quality, while recall [34] values are larger than those of the baseline for all compared patch sizes. This demonstrates that retrieval-augmented models maintain high sample diversity and conditioning on global object attributes yields more coherent samples than only using object parts in the database.

Increasing dataset complexity. To investigate its versatility for more complex generative tasks, we now compare our model to its fully-parametric counterpart when systematically increasing the complexity of the data distribution $p(x)$. For both approaches, we train three identical models on the dogs-, mammals- and animals-subsets of ImageNet [10], cf. Tab. 3, until convergence and thereafter assess performance metrics [19, 34].

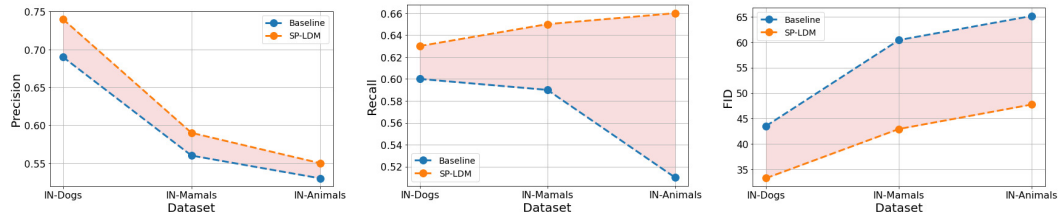


Figure 9: Assessing benefits of our proposed semi-parametric approach when increasing dataset complexity. Starting with the dog-subset of ImageNet [10], we gradually increase the number of used classes, thus what results in more complex generative tasks. We observe FID- and recall-gaps between a *RDM* and a fully-parametric equivalent model increases for more complex datasets as indicated by the shaded areas. Remarkably, the recall score of *RDM* increases with increasing complexity, while strongly degrades for the baseline.

Fig. 9 visualizes the results. Even for low-complexity datasets such as *IN-Dogs*, *RDM* improves over a standard *LDM*. For more complex datasets, the performance gains become more significant, except for precision, where the gap is approximately constant. Interestingly, the recall score of *RDM* improves with increasing complexity, while that of the baseline strongly degrades. We attribute this to the explicit access of *RDM* to nearby visual instances for all classes including underrepresented

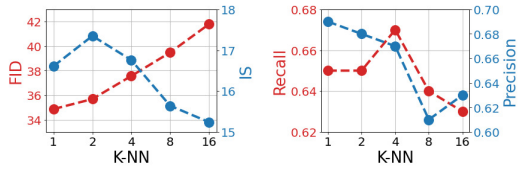


Figure 7: Influence of number of nearest neighbors during training.

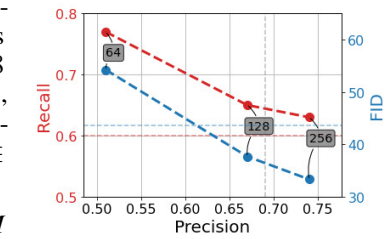


Figure 8: Effect of patch size of images in the retrieval database.

ones via the proposal distribution $p_{\mathcal{D}}(\tilde{x})$, *cf.* Eq. (4), whereas a standard *LDM* might focus only on the modes containing the most often occurring classes.

4.2 Image Generation with Retrieval-Augmented Diffusion Models

Unconditional Image Generation By choosing appropriate parameters based on the analysis from Sec. 4.1 we obtain a strong image generator. Fig. 5 shows samples from our model trained on the ImageNet [10] dataset for different sets $\mathcal{M}_{\mathcal{D}}^{(k)}(\tilde{x})$ of retrieved neighbors given a pseudo-query $\tilde{x} \sim p_{\mathcal{D}}(\tilde{x})$. We also plot the nearest neighbors from the train set to show that it is actually disjoint from the database \mathcal{D} .

Conditional Image Generation without Conditional Training As presented in Sec. 3.3 *RDM* can flexibly adapt to conditional inference tasks, which is beneficial since annotating vast amounts of data required during training can be costly.

In Fig. 2, we show the zero-shot text-to-image synthesis capabilities of our ImageNet model for user defined text prompts. When building the set $\mathcal{M}_{\mathcal{D}}^{(k)}(c_{\text{text}})$ by directly using the CLIP encodings $\phi_{\text{CLIP}}(c_{\text{text}})$ of the actual textual description itself (top row), we interestingly see that our model generalizes to generating fictional descriptions and transferring attributions across object classes. However, when using $\phi_{\text{CLIP}}(c_{\text{text}})$ together with its $k - 1$ nearest neighbors from the database \mathcal{D} as done in [1], the model does not generalize to these difficult conditional inputs (mid row). When omitting the text representation and only using the k CLIP image representations of the nearest neighbors, the results get even worse (bottom row). We hypothesize that further scaling the train dataset of such a retrieval-augmented model and applying the text-only strategy shown in the top row can lead to a strong text-to-image model which does not need paired text/image data during training.

Similarly we can apply our model to zero-shot class-conditional image synthesis as proposed in Sec. 3.3. Fig. 10 shows samples from our model for classes from ImageNet.

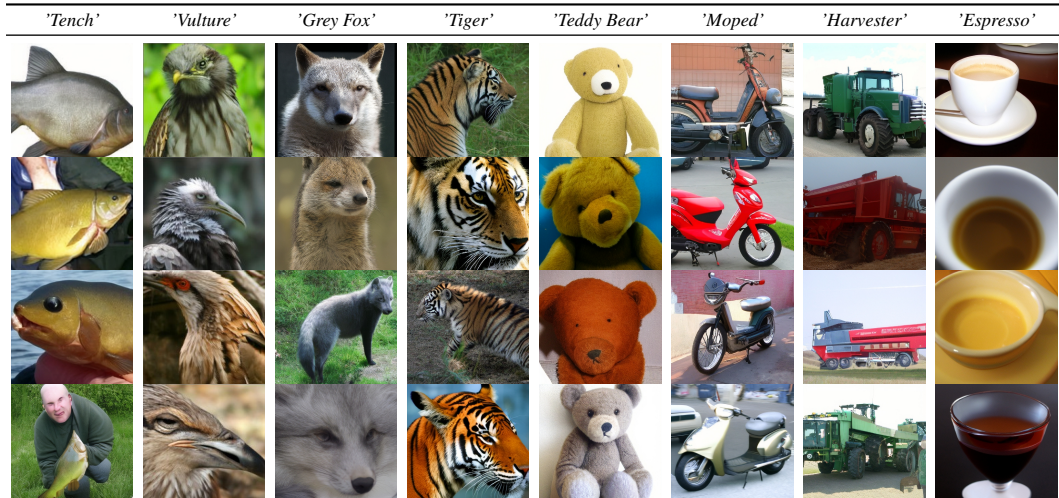


Figure 10: *RDM* can be used for class-conditional generation on ImageNet despite being trained without class labels. To achieve this, we compute a pool of nearby visual instances from the database \mathcal{D} for each class label based on its textual description, and combine it with its $k - 1$ nearest neighbors as conditioning.

4.3 Sampling Strategies

Top-m sampling. In this section, we evaluate the effects of the *top-m sampling* strategy introduced in Sec. 3.3. We train a *RDM* on the ImageNet [10] dataset and conduct the usual generative performance metrics based on 50k generated samples and the entire training set [3]. The obtained results are shown in Fig. 12a. For precision and recall scores, we observe a truncation behavior similar to other inference-time sampling techniques [3, 11, 20, 15]: For small values of m , we obtain coherent samples, which all come from a single or a small number of modes, as indicated by large precision

Single Example	$m = 10^{-5}$	$m = 10^{-4}$	$m = 10^{-3}$	$m = 10^{-2}$
				
				
				
				
				

Figure 11: Visual examples on the quality-diversity trade off obtained by *top- m sampling*. For heavily truncated $p_{\mathcal{D}}(\tilde{x})$ we obtain extremely low sample diversity as visualized in the examples on the left part. Increasing m results in more diversity but lower sample fidelity (right part). All images generated with guidance scale $s = 1.5$ and 100 DDIM steps.

scores. Increasing m , on the other hand, boosts diversity at the expense of consistency. For FID and IS, we interestingly find a sweet spot for $m = 0.01$, which yields optima for both of these metrics. Visual examples for different values of m are shown in Fig. 11.

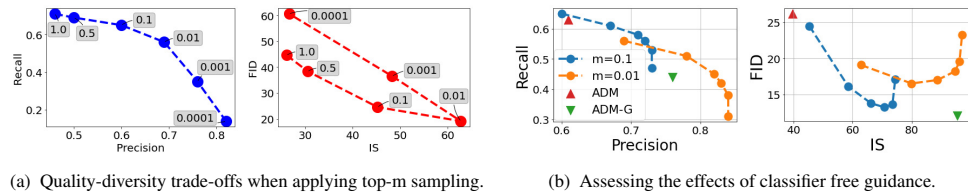


Figure 12: Analysis of the quality-diversity trade-offs when applying top- m sampling and classifier-free guidance.

Neighbors	$s = 1$	$s = 2$	$s = 3$	$s = 4$

Figure 13: Visualizing the effects of retrieval based classifier free guidance. All images generated with fixed random seed, $m = 0.1$ and 100 DDIM steps.

Classifier-free guidance. Since our decoding head p_θ is a conditional diffusion model (conditioned on the neighbor encodings $\phi(y)$), we can apply classifier-free diffusion guidance [20]. Interestingly, we find that we can apply this technique without adding an additional \emptyset -label to account for a purely unconditional setting while training ϵ_θ , as originally proposed in [20]. Instead we simply use a vector of zeros to generate an unconditional prediction with ϵ_θ in each diffusion time step during inference. Additionally, this technique can be combined with *top-m sampling* to obtain further control during sampling. In Fig. 12b we show the effects of this combination for the ImageNet-model as described in the previous paragraph, with $m \in \{0.01, 0.1\}$ and classifier scale $s \in \{1.0, 1.25, 1.5, 1.75, 2.0, 3.0\}$, from left to right for each line. Moreover we qualitatively show the effects of guidance in Fig. 13.

4.4 Comparison with State of the Art

Per the analysis presented in Sec. 4.1, we identify implementing ϕ as a pre-trained CLIP [40] model using $H_D = W_D = 256$ and retrieving $k = 4$ nearest neighbors to be suitable design choices of our proposed *RDM*. Using these options, we quantitatively compare its performance with the recent state-of-the-art diffusion model ADM [11] and the GAN-based model IC-GAN [5], which requires access to the training set examples during inference and consequently evaluates only on the validation set, in unconditional image synthesis on ImageNet [10] 256×256 , *cf.* Tab. 1. With

Method	FID \downarrow		IS \uparrow	Precision \uparrow	Recall \uparrow	Nparams
	train	val				
IC-GAN [5]	-	15.60*	59.00*	-	-	conditioned on train set, add. aug.
ADM [11]	26.21	32.50*	39.70	0.61	0.63	554M 250 steps
ADM-G [11]	33.03	-	32.92	0.56	0.65	618M 250 steps, c.g., s=1.0
ADM-G [11]	12.00	-	95.41	0.76	0.44	618M 250 steps, c.g., s=10.0
<i>RDM</i> -4 (ours)	24.50	21.28	45.29	0.60	0.65	400M 100 steps, $m = 0.1$
<i>RDM</i> -4 (ours)	19.08	16.89	62.78	0.57	0.56	400M 100 steps, $m = 0.01$
<i>RDM</i> -4 (ours)	13.22	<u>12.29</u>	70.64	0.72	0.56	400M 100 steps, c.f.g., $s = 1.75, m = 0.1$
<i>RDM</i> -4 (ours)	13.60	13.11	87.58	0.79	0.51	400M 100 steps, c.f.g., $s = 1.5, m = 0.02$
<i>RDM</i> -4 (ours)	12.21	11.31	77.93	0.75	0.55	400M 100 steps, c.f.g., $s = 1.5, m = 0.05$

Table 1: Comparison of *RDM* with recent state-of-the-art methods for unconditional image generation on ImageNet [10]. While *c.f.g.* denotes classifier-free guidance with a scale parameter s as proposed in [20], *c.g.* refers to classic diffusion guidance [11], what requires a classifier pretrained on the noisy representations of diffusion models to be available. Precision and recall metrics are computed with respect to the training set. *: numbers taken from [5].

classifier-free guidance, our model attains better scores than IC-GAN and ADM while being on par with ADM-G [11] which requires an additional classifier and the labels of training instances. Without any additional information about training data e.g. image labels, *RDM* achieves the best overall performance considering all the metrics with less parameters than ADM.

For $m = 0.1$, our retrieval-augmented *RDM* clearly surpasses the state-of-the art unconditional model ADM for FID, IS, precision and, with no guidance, also for recall. For $s = 1.75$, we observe bisected FID scores compared to our unguided model and even reach the guided model ADM-G, which, unlike *RDM*, requires a classifier that is pre-trained on noisy data representations. Such large effects for classifier-free guidance [20] are in contrast to [42], where this technique is found to be not as effective.

When intending to emphasize diversity, higher values for m and no guidance are suitable choices for *RDM*. Using these parameters ($m = 0.1$), our model improves in recall over ADM while still yielding better FID scores. For fixed m and increasing values of s , we qualitatively observe the same quality-diversity trade-off as for standard classifier guidance. The same trade-off can also be achieved with decreasing values of m . When $m = 0.01$ our guided model does not reach similar recall and FID values as for larger m , due to reduced diversity, but the model still yields good performance in terms of precision, recall and IS for suitable choices of s . The optimal parameters for FID are $m = 0.05$, $s = 1.5$, as visualized at the bottom row of Tab. 1.

5 Conclusion

This paper explores the effects of conditioning diffusion models for image synthesis on retrieved representations from an external database \mathcal{D} . In particular, we analyze the effect on training tasks of varying complexity, and find gains especially for more complex, multi-modal datasets. Our experiments show that CLIP both serves as an efficient retrieval model *and* provides good representations for conditioning the denoising diffusion model, although other choices such as discrete embeddings are possible. Our model produces high-quality samples and can be flexibly employed for conditional tasks such as text-to-image synthesis, despite being trained on images only.

It is also easy to implement: Given a sufficiently large database \mathcal{D} , which is readily available via collections of non-curated image-only data, pre-computation of the neighbors via an optimized retrieval codebase (ScaNN) is fast. Furthermore, when using CLIP embeddings as the retrieved representations $\phi = \phi_{\text{CLIP}}$, the retrieval database can be interpreted and stored as a standard embedding layer of size $|\mathcal{D}| \times 512$.

While the synthesis quality and the flexibility of control at test time is already high, some open questions remain: For example, how does the composition of \mathcal{D} influence the results? Is it possible to build a hierarchy from different \mathcal{D}_i , holding exemplars of varying size and/or scale? Can existing, classic diffusion models such as ADM [11] be fine-tuned into retrieval-augmented models, similar to [2]? Can larger CLIP backbones further boost the performance? Can guided image synthesis [9] benefit from an explicit database available during synthesis?

We hope that future research can answer these questions and scale this approach to very large datasets beyond ImageNet scale; and apply our framework to other types of generative models.

Appendix

A Implementation Details

A.1 Training Details

In Tab. 2 we show the hyperparameters which were used to train the models presented in this work. For the retrieval-augmented models, the hyperparameters correspond only to the decoding head, as the other parts of the model are not trainable. We trained our main model (which was used to generate all qualitative results in this work as well as the quantitative results shown in Tab. 1) on eight NVIDIA A-100-SXM4 with 80GB RAM per GPU. The models from the analysis in Sec. 4.1 are all trained on a single NVIDIA A-100 GPU with 40GB RAM. To train the *LDM* baselines with the same batch size as the corresponding *RDM*, we use gradient checkpointing [8] which reduces memory cost during backpropagation at the expense of additional computations in the forward pass. As these baselines are 'common' unconditional models, we use self-attention (SA) instead of the cross-attention layers (CA) which are used to feed the nearest neighbor representation ϕ to the decoding head of the semi-parametric models. All our models are implemented in PyTorch. We will release the code and pretrained models in the near future.

	<i>RDM</i> [*]	<i>RDM</i> [†]	baseline <i>LDM</i> [†]
Dataset	ImageNet	ImageNet-subsets, cf. Tab. 3	ImageNet-subsets, cf. Tab. 3
z -shape	$64 \times 64 \times 3$	$64 \times 64 \times 3$	$64 \times 64 \times 3$
$ \mathcal{Z} $	8192	8192	8192
Diffusion steps	1000	1000	1000
Noise Schedule	linear	linear	linear
Model Size	400M	400M	576M
Channels	192	192	224
Depth	2	2	2
Channel Multiplier	1,2,3,5	1,2,3,5	1,2,4,6
BigGAN [3] up/downsampling	✗	✗	✓
activation rescaling [55, 26, 27]	✗	✗	✓
Number of Heads	32	32	32
Batch Size	1240	56	56
Iterations	112K	subset dependent [‡]	subset dependent [‡]
Learning Rate	1.0e-4	1.0e-4	1.0e-4
Conditioning	CA	CA	-
CA/SA-resolutions	32, 16, 8	32, 16, 8	32, 16, 8
Embedding Dimension	512	512 ($\phi = \phi_{\text{CLIP}}/1024$ ($\phi = \phi_{\text{VQGAN}}$))	-
Transformers Depth	1	1	-

Table 2: Hyperparameters for the models used in this work.^{*}: All qualitative examples in this work and the numbers presented in Tab. 1 are generated with this model.[†]: The various semi- and fully-parametric models referred to in Sec. 4.1 are trained with these hyperparameters;[‡]: All models were trained until convergence.

Statistics for ImageNet subsets In Tab. 3 we present detailed statistics for the datasets involved in the comparison of fully- and semi-parametric generative models for increasing complexity of the modeled data distribution. For the dogs subset, we used the class labels ranging from 181 to 280, resulting in a training dataset containing $M = 163K$ examples. Including all mammals lead to overall 241 classes with $M = 309K$ examples whereas training on all 398 classes referring to animals resulted in a dataset of $M = 511K$ individual images. As for our main experiments, we did not use any class labels for training the models on these datasets.

Dataset	class labels	M
IN-dogs	181-280	163K
IN-mammals	147-388	309K
IN-animals	0-397	511K

Table 3: Statistics for the ImageNet subsets used in the analysis on dataset complexity in Sec. 4.1 and Fig. 9.

A.2 Evaluation Details

Analysis Experiments from Sec. 4.1 To generate the results shown in the analysis presented Sec. 4.1 we used $m = 0.01$ and no unconditional guidance for all compared configurations in each of the different sub-analyses. For the comparison regarding different encoders ϕ to obtain suitable

representations for the retrieved neighbors, we use a $f - 16$ VQGAN pretrained on OpenImages from Rombach et al [44]⁴. To limit the dimensionality of the representation we resize the input images for each of the $k = 4$ nearest neighbors to 128×128 px, as this does not hurt the model’s performance, resulting in a latent tensor of shape $8 \times 8 \times 256$. We then form a sequence shape 64×256 for each nearest neighbor representation by applying raster scan reordering [59] and subsequently concatenate all $k = 4$ individual representation channel-wise, which gives us the final conditioning input for the decoding head with a shape of 64×1024 .

Comparison with State of the Art For the SOTA comparison presented in Sec. 4.4, we used the evaluation protocol proposed in ADM [11]. We also used their publicly available evaluation pipeline⁵.

B Additional Samples

We show additional samples for zero-shot text-to-image synthesis in Fig. 14 and additional unconditional ImageNet samples in Fig. 15.

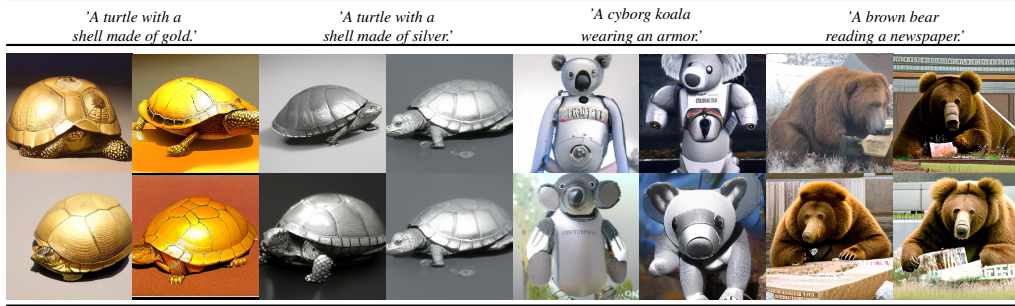


Figure 14: Additional zero-shot text to image samples from our model as in Fig. 2.

⁴<https://github.com/CompVis/latent-diffusion>

⁵<https://github.com/openai/guided-diffusion>

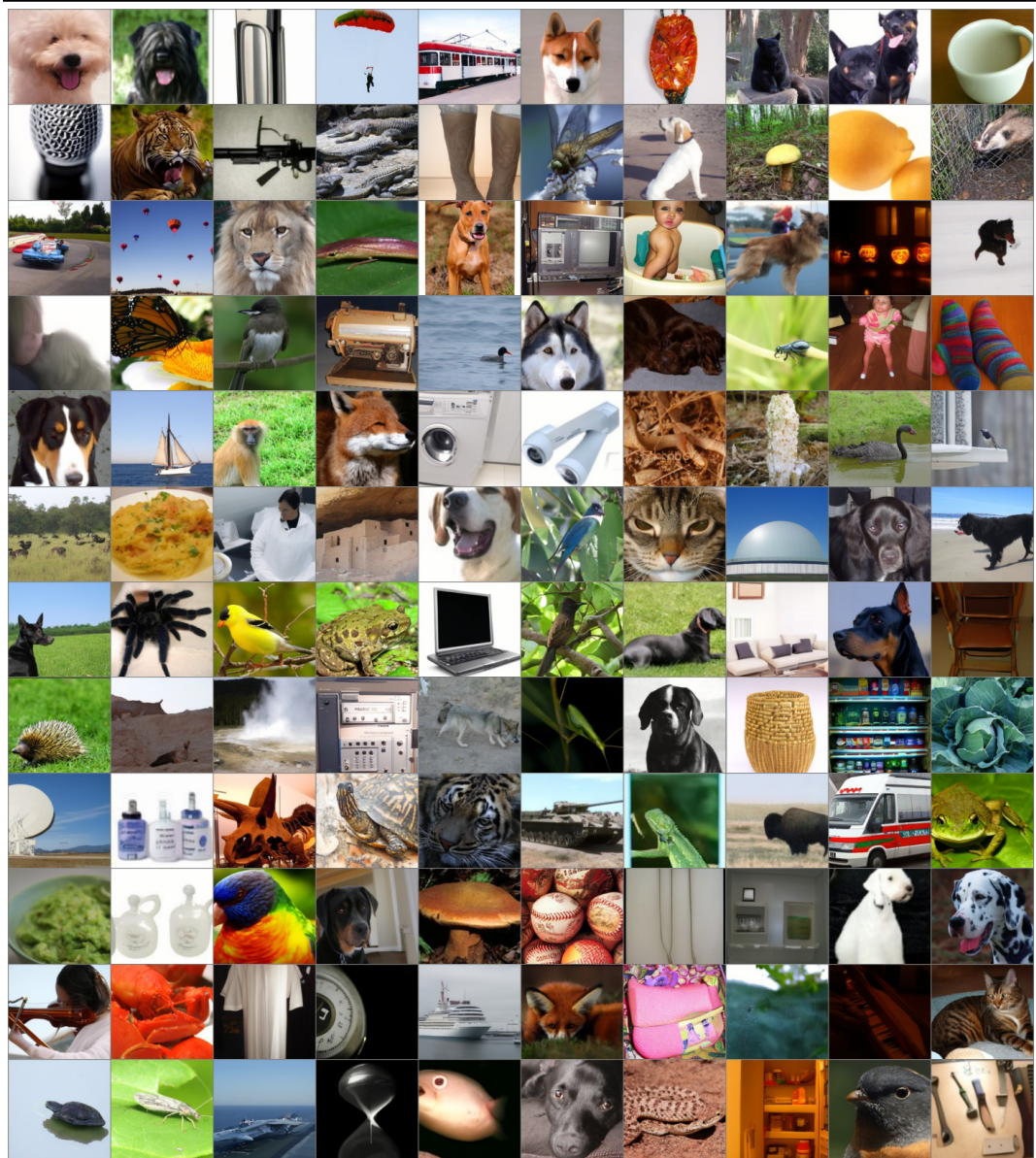


Figure 15: Random samples from our RDM , with $m = 0.01$ and classifier-free guidance with $s = 2.0$. Samples were generated with 100 DDIM steps.

References

- [1] Oron Ashual, Shelly Sheynin, Adam Polyak, Uriel Singer, Oran Gafni, Eliya Nachmani, and Yaniv Taigman. Knn-diffusion: Image generation via large-scale retrieval. *arXiv preprint arXiv:2204.02849*, 2022.
- [2] Sebastian Borgeaud, Arthur Mensch, Jordan Hoffmann, Trevor Cai, Eliza Rutherford, Katie Millican, George van den Driessche, Jean-Baptiste Lespiau, Bogdan Damoc, Aidan Clark, et al. Improving language models by retrieving from trillions of tokens. *arXiv preprint arXiv:2112.04426*, 2021.
- [3] Andrew Brock, Jeff Donahue, and Karen Simonyan. Large scale gan training for high fidelity natural image synthesis. *arXiv preprint arXiv:1809.11096*, 2018.
- [4] Tom Brown, Benjamin Mann, Nick Ryder, Melanie Subbiah, Jared D Kaplan, Prafulla Dhariwal, Arvind Neelakantan, Pranav Shyam, Girish Sastry, Amanda Askell, et al. Language models are few-shot learners. *Advances in neural information processing systems*, 33:1877–1901, 2020.
- [5] Arantxa Casanova, Marlène Careil, Jakob Verbeek, Michal Drozdzal, and Adriana Romero Soriano. Instance-conditioned gan. *Advances in Neural Information Processing Systems*, 34, 2021.
- [6] Lucy Chai, Michael Gharbi, Eli Shechtman, Phillip Isola, and Richard Zhang. Any-resolution training for high-resolution image synthesis. *arXiv preprint arXiv:2204.07156*, 2022.
- [7] Mark Chen, Alec Radford, Rewon Child, Jeffrey Wu, Heewoo Jun, David Luan, and Ilya Sutskever. Generative pretraining from pixels. In *International Conference on Machine Learning*, pages 1691–1703. PMLR, 2020.
- [8] Tianqi Chen, Bing Xu, Chiyuan Zhang, and Carlos Guestrin. Training deep nets with sublinear memory cost. *ArXiv*, abs/1604.06174, 2016.
- [9] Katherine Crowson, Stella Biderman, Daniel Kornis, Dashiell Stander, Eric Hallahan, Louis Castricato, and Edward Raff. Vqgan-clip: Open domain image generation and editing with natural language guidance, 2022. URL <https://arxiv.org/abs/2204.08583>.
- [10] Jia Deng, Wei Dong, Richard Socher, Li-Jia Li, Kai Li, and Li Fei-Fei. Imagenet: A large-scale hierarchical image database. In *2009 IEEE conference on computer vision and pattern recognition*, pages 248–255. Ieee, 2009.
- [11] Prafulla Dhariwal and Alexander Nichol. Diffusion models beat gans on image synthesis. *Advances in Neural Information Processing Systems*, 34, 2021.
- [12] Alexey Dosovitskiy, Lucas Beyer, Alexander Kolesnikov, Dirk Weissenborn, Xiaohua Zhai, Thomas Unterthiner, Mostafa Dehghani, Matthias Minderer, Georg Heigold, Sylvain Gelly, et al. An image is worth 16x16 words: Transformers for image recognition at scale. *arXiv preprint arXiv:2010.11929*, 2020.
- [13] Patrick Esser, Robin Rombach, Andreas Blattmann, and Bjorn Ommer. Imagebart: Bidirectional context with multinomial diffusion for autoregressive image synthesis. *Advances in Neural Information Processing Systems*, 34, 2021.
- [14] Patrick Esser, Robin Rombach, and Bjorn Ommer. Taming transformers for high-resolution image synthesis. In *Proceedings of the IEEE/CVF Conference on Computer Vision and Pattern Recognition*, pages 12873–12883, 2021.
- [15] Angela Fan, Mike Lewis, and Yann N. Dauphin. Hierarchical neural story generation. *CoRR*, abs/1805.04833, 2018. URL <http://arxiv.org/abs/1805.04833>.
- [16] Shuyang Gu, Dong Chen, Jianmin Bao, Fang Wen, Bo Zhang, Dongdong Chen, Lu Yuan, and Baining Guo. Vector quantized diffusion model for text-to-image synthesis. *arXiv preprint arXiv:2111.14822*, 2021.
- [17] Ruiqi Guo, Philip Sun, Erik Lindgren, Quan Geng, David Simcha, Felix Chern, and Sanjiv Kumar. Accelerating large-scale inference with anisotropic vector quantization. In Hal Daumé III and Aarti Singh, editors, *Proceedings of the 37th International Conference on Machine Learning*, volume 119 of *Proceedings of Machine Learning Research*, pages 3887–3896. PMLR, 13–18 Jul 2020. URL <https://proceedings.mlr.press/v119/guo20h.html>.
- [18] Kelvin Guu, Kenton Lee, Zora Tung, Panupong Pasupat, and Mingwei Chang. Retrieval augmented language model pre-training. In *International Conference on Machine Learning*, pages 3929–3938. PMLR, 2020.
- [19] Martin Heusel, Hubert Ramsauer, Thomas Unterthiner, Bernhard Nessler, and Sepp Hochreiter. Gans trained by a two time-scale update rule converge to a local nash equilibrium. In *Adv. Neural Inform. Process. Syst.*, pages 6626–6637, 2017.
- [20] Jonathan Ho and Tim Salimans. Classifier-free diffusion guidance. In *NeurIPS 2021 Workshop on Deep Generative Models and Downstream Applications*, 2021.
- [21] Jonathan Ho, Ajay Jain, and Pieter Abbeel. Denoising diffusion probabilistic models. *Advances in Neural Information Processing Systems*, 33:6840–6851, 2020.

[22] Jonathan Ho, Chitwan Saharia, William Chan, David J Fleet, Mohammad Norouzi, and Tim Salimans. Cascaded diffusion models for high fidelity image generation. *Journal of Machine Learning Research*, 23(47):1–33, 2022.

[23] Jonathan Ho, Tim Salimans, Alexey Gritsenko, William Chan, Mohammad Norouzi, and David J Fleet. Video diffusion models. *arXiv preprint arXiv:2204.03458*, 2022.

[24] Emiel Hoogeboom, Victor Garcia Satorras, Clément Vignac, and Max Welling. Equivariant diffusion for molecule generation in 3d. *arXiv preprint arXiv:2203.17003*, 2022.

[25] Jared Kaplan, Sam McCandlish, Tom Henighan, Tom B. Brown, Benjamin Chess, Rewon Child, Scott Gray, Alec Radford, Jeffrey Wu, and Dario Amodei. Scaling laws for neural language models. *CoRR*, abs/2001.08361, 2020.

[26] Tero Karras, Samuli Laine, and Timo Aila. A style-based generator architecture for generative adversarial networks. In *Proceedings of the IEEE/CVF conference on computer vision and pattern recognition*, pages 4401–4410, 2019.

[27] Tero Karras, Samuli Laine, Miika Aittala, Janne Hellsten, Jaakko Lehtinen, and Timo Aila. Analyzing and improving the image quality of stylegan. In *Proceedings of the IEEE/CVF conference on computer vision and pattern recognition*, pages 8110–8119, 2020.

[28] Tero Karras, Miika Aittala, Samuli Laine, Erik Härkönen, Janne Hellsten, Jaakko Lehtinen, and Timo Aila. Alias-free generative adversarial networks. *Advances in Neural Information Processing Systems*, 34, 2021.

[29] Urvashi Khandelwal, Omer Levy, Dan Jurafsky, Luke Zettlemoyer, and Mike Lewis. Generalization through memorization: Nearest neighbor language models. *arXiv preprint arXiv:1911.00172*, 2019.

[30] Urvashi Khandelwal, Angela Fan, Dan Jurafsky, Luke Zettlemoyer, and Mike Lewis. Nearest neighbor machine translation. *arXiv preprint arXiv:2010.00710*, 2020.

[31] Diederik P Kingma, Tim Salimans, Ben Poole, and Jonathan Ho. Variational diffusion models. *arXiv preprint arXiv:2107.00630*, 2021.

[32] Zhifeng Kong, Wei Ping, Jiaji Huang, Kexin Zhao, and Bryan Catanzaro. Diffwave: A versatile diffusion model for audio synthesis. *arXiv preprint arXiv:2009.09761*, 2020.

[33] Alina Kuznetsova, Hassan Rom, Neil Alldrin, Jasper R. R. Uijlings, Ivan Krasin, Jordi Pont-Tuset, Shahab Kamali, Stefan Popov, Matteo Mallochi, Tom Duerig, and Vittorio Ferrari. The open images dataset V4: unified image classification, object detection, and visual relationship detection at scale. *CoRR*, abs/1811.00982, 2018. URL <http://arxiv.org/abs/1811.00982>.

[34] Tuomas Kynkääniemi, Tero Karras, Samuli Laine, Jaakko Lehtinen, and Timo Aila. Improved precision and recall metric for assessing generative models. *CoRR*, abs/1904.06991, 2019. URL <http://arxiv.org/abs/1904.06991>.

[35] Luping Liu, Yi Ren, Zhijie Lin, and Zhou Zhao. Pseudo numerical methods for diffusion models on manifolds. *CoRR*, abs/2202.09778, 2022. URL <https://arxiv.org/abs/2202.09778>.

[36] Alexander Long, Wei Yin, Thalaiyasingam Ajanthan, Vu Nguyen, Pulak Purkait, Ravi Garg, Alan Blair, Chunhua Shen, and Anton van den Hengel. Retrieval augmented classification for long-tail visual recognition. *arXiv preprint arXiv:2202.11233*, 2022.

[37] Eric Luhman and Troy Luhman. Knowledge distillation in iterative generative models for improved sampling speed. *CoRR*, abs/2101.02388, 2021. URL <https://arxiv.org/abs/2101.02388>.

[38] Yuxian Meng, Shi Zong, Xiaoya Li, Xiaofei Sun, Tianwei Zhang, Fei Wu, and Jiwei Li. Gnn-lm: Language modeling based on global contexts via gnn. *arXiv preprint arXiv:2110.08743*, 2021.

[39] Alex Nichol, Prafulla Dhariwal, Aditya Ramesh, Pranav Shyam, Pamela Mishkin, Bob McGrew, Ilya Sutskever, and Mark Chen. Glide: Towards photorealistic image generation and editing with text-guided diffusion models. *arXiv preprint arXiv:2112.10741*, 2021.

[40] Alec Radford, Jong Wook Kim, Chris Hallacy, Aditya Ramesh, Gabriel Goh, Sandhini Agarwal, Girish Sastry, Amanda Askell, Pamela Mishkin, Jack Clark, et al. Learning transferable visual models from natural language supervision. In *International Conference on Machine Learning*, pages 8748–8763. PMLR, 2021.

[41] Aditya Ramesh, Mikhail Pavlov, Gabriel Goh, Scott Gray, Chelsea Voss, Alec Radford, Mark Chen, and Ilya Sutskever. Zero-shot text-to-image generation. In *International Conference on Machine Learning*, pages 8821–8831. PMLR, 2021.

[42] Aditya Ramesh, Prafulla Dhariwal, Alex Nichol, Casey Chu, and Mark Chen. Hierarchical text-conditional image generation with clip latents. *arXiv preprint arXiv:2204.06125*, 2022.

[43] Ali Razavi, Aaron Van den Oord, and Oriol Vinyals. Generating diverse high-fidelity images with vq-vae-2. *Advances in neural information processing systems*, 32, 2019.

[44] Robin Rombach, Andreas Blattmann, Dominik Lorenz, Patrick Esser, and Björn Ommer. High-resolution image synthesis with latent diffusion models. *arXiv preprint arXiv:2112.10752*, 2021.

[45] Olaf Ronneberger, Philipp Fischer, and Thomas Brox. U-net: Convolutional networks for biomedical image segmentation. In *MICCAI (3)*, volume 9351 of *Lecture Notes in Computer Science*, pages 234–241. Springer, 2015.

[46] Chitwan Saharia, Jonathan Ho, William Chan, Tim Salimans, David J Fleet, and Mohammad Norouzi. Image super-resolution via iterative refinement. *arXiv preprint arXiv:2104.07636*, 2021.

[47] Tim Salimans and Jonathan Ho. Progressive distillation for fast sampling of diffusion models. *CoRR*, abs/2202.00512, 2022. URL <https://arxiv.org/abs/2202.00512>.

[48] Tim Salimans, I. Goodfellow, Wojciech Zaremba, Vicki Cheung, Alec Radford, and Xi Chen. Improved techniques for training gans. In *NIPS*, 2016.

[49] Axel Sauer, Katja Schwarz, and Andreas Geiger. Stylegan-xl: Scaling stylegan to large diverse datasets. *arXiv preprint arXiv:2202.00273*, 2022.

[50] Yawar Siddiqui, Justus Thies, Fangchang Ma, Qi Shan, Matthias Nießner, and Angela Dai. Retrievalfuse: Neural 3d scene reconstruction with a database. In *Proceedings of the IEEE/CVF International Conference on Computer Vision*, pages 12568–12577, 2021.

[51] Abhishek Sinha, Jiaming Song, Chenlin Meng, and Stefano Ermon. D2C: diffusion-denoising models for few-shot conditional generation. *CoRR*, abs/2106.06819, 2021. URL <https://arxiv.org/abs/2106.06819>.

[52] Jascha Sohl-Dickstein, Eric Weiss, Niru Maheswaranathan, and Surya Ganguli. Deep unsupervised learning using nonequilibrium thermodynamics. In *International Conference on Machine Learning*, pages 2256–2265. PMLR, 2015.

[53] Jiaming Song, Chenlin Meng, and Stefano Ermon. Denoising diffusion implicit models. *arXiv preprint arXiv:2010.02502*, 2020.

[54] Yang Song and Stefano Ermon. Generative modeling by estimating gradients of the data distribution. *Advances in Neural Information Processing Systems*, 32, 2019.

[55] Yang Song, Jascha Sohl-Dickstein, Diederik P. Kingma, Abhishek Kumar, Stefano Ermon, and Ben Poole. Score-based generative modeling through stochastic differential equations. *CoRR*, abs/2011.13456, 2020.

[56] Rich Sutton. The bitter lesson, 2019. URL <http://www.incompleteideas.net/IncIdeas/BitterLesson.html>.

[57] Hung-Yu Tseng, Hsin-Ying Lee, Lu Jiang, Ming-Hsuan Yang, and Weilong Yang. Retrievegan: Image synthesis via differentiable patch retrieval. In *European Conference on Computer Vision*, pages 242–257. Springer, 2020.

[58] Arash Vahdat, Karsten Kreis, and Jan Kautz. Score-based generative modeling in latent space. *Advances in Neural Information Processing Systems*, 34, 2021.

[59] Aaron Van Den Oord, Oriol Vinyals, et al. Neural discrete representation learning. *Advances in neural information processing systems*, 30, 2017.

[60] Ashish Vaswani, Noam Shazeer, Niki Parmar, Jakob Uszkoreit, Llion Jones, Aidan N Gomez, Łukasz Kaiser, and Illia Polosukhin. Attention is all you need. *Advances in neural information processing systems*, 30, 2017.

[61] Zhisheng Xiao, Karsten Kreis, and Arash Vahdat. Tackling the generative learning trilemma with denoising diffusion gans. *arXiv preprint arXiv:2112.07804*, 2021.

[62] Minkai Xu, Lantao Yu, Yang Song, Chence Shi, Stefano Ermon, and Jian Tang. Geodiff: A geometric diffusion model for molecular conformation generation. *arXiv preprint arXiv:2203.02923*, 2022.

[63] Rui Xu, Minghao Guo, Jiaqi Wang, Xiaoxiao Li, Bolei Zhou, and Chen Change Loy. Texture memory-augmented deep patch-based image inpainting. *IEEE Transactions on Image Processing*, 30:9112–9124, 2021.

[64] Ruihan Yang, Prakhar Srivastava, and Stephan Mandt. Diffusion probabilistic modeling for video generation. *arXiv preprint arXiv:2203.09481*, 2022.